Magnetic susceptibilities, critical fields, and critical currents of Co- and Zn-doped $YBa_2Cu_3O_7$

D. N. Zheng, A. M. Campbell, J. D. Johnson, J. R. Cooper, F. J. Blunt, A. Porch,* and P. A. Freeman
*Interdisciplinary Research Centre in Superconductivity, University of Cambridge, Madingley Road, Cambridge CB3 0HE,
United Kingdom*

We have performed ac susceptibility, dc magnetization, and critical-current measurements on a series of $YBa_2Cu_3O_7$ samples with low levels of Co and Zn doping. The anisotropic superconducting properties were studied by magnetically aligning the powders in wax. By combining previous results of the magnetic penetration depth λ with the thermodynamic critical field H_c data, obtained from previous specific-heat measurements, we were able to estimate the coherence length ξ, the lower and upper critical fields H_{c1} and H_{c2}, and the Ginzbug-Landau parameter κ of these samples. We have compared these estimates with values determined from dc magnetization curves near T_c. Both intra- and intergrain critical current densities, $J_{c(intra)}$ and $J_{c(inter)}$, were measured magnetically on bulk samples and found to decrease with Co and Zn doping. In particular, the ratio of $J_{c(intra)}$ and $J_{c(inter)}$ was found to be insensitive to doping, although the coherence length was increased in the doped samples. Moreover, $J_{c(intra)}$ correlates well with the condensation energies of the samples. This indicates that doping with Co or Zn weakens the energy barrier of the existing pinning sites and has a negative overall effect on the ability of $YBa_2Cu_3O_7$ to carry loss-free currents. Finally, the results of irreversibility line measurements show that the Co substitution, occurring in the CuO chain sites, has a more severe effect than Zn substitution, occurring in the CuO_2 plane sites, because of the increased anisotropy.

I. INTRODUCTION

Flux pinning and critical-current density J_c are the most important properties needed for practical applications of high-T_c superconductors. It is well known that these two properties are closely linked to fundamental superconducting properties[1] such as the coherence length ξ, the magnetic penetration depth λ, and the critical fields H_c, H_{c1}, and H_{c2}. Therefore, to understand and improve the J_c behavior of high-T_c superconductors, systematic and correlated studies involving both J_c and the basic superconducting parameters are needed. Here we report values of λ, ξ, H_{c1}, H_{c2}, and J_c measured on a series of $YBa_2Cu_3O_7$ (YBCO) samples with low-level Co and Zn doping, in an attempt to draw some conclusions about the correlation between them, and also to investigate the effect of partial substitution of Cu.

Additionally, the basic properties of a superconductor provide insight into the superconducting mechanism. However, there are difficulties in properly determining these fundamental quantities due to a number of reasons. For example, because of the large value of H_{c2}, it can only be measured at temperatures near to T_c, where thermal fluctuation effects are more significant so that the error in the determination of H_{c2} can be large. In the present work, by making use of the values of the penetration depth obtained from ac susceptibility data[2] and the values of the thermodynamic critical field determined from specific-heat measurements,[3,4] we are able to determine other parameters using the Ginzburg-Landau relations. This way provides the advantage that these parameters can be evaluated over a wide temperature range from T_c to a temperature close to 0 K. Although the

Ginzburg-Landau theory is strictly valid only close to T_c, it is found to be a reasonable approximation well below T_c.[5,6]

The material parameters or properties of $YBa_2Cu_3O_7$ can be systematically changed by partial substitution of Cu with another element. Transition metals with $3d$ electrons, such as Fe, Co, Ni, Zn, are often used as dopants because the Cu $3d$ electrons are believed to be relevant to the superconductivity.[7-9] In this work we chose trivalent Co and divalent Zn as dopants. The positions of Co and Zn for Cu within the crystal lattice of YBCO have been studied by x-ray diffraction,[10] neutron diffraction,[11,12] and thermogravimetric analysis.[11] It is generally agreed that Co ions primarily substitute for the chain Cu(1) sites. In the case of Zn doping, although there is no firm consensus in literature regarding the substitution site of the Zn ions,[13-15] it is plausible to believe that at least some (probably all) Zn ions occupy Cu(2) sites in the CuO_2 plane. It would be hard to explain the strong suppression of T_c by Zn doping if Zn ions go only to chain sites. We shall show that because of their different substituting sites Co and Zn affect the properties of YBCO differently.

II. EXPERIMENT

Polycrystalline samples with a compositional formula of $YBa_2(Cu_{1-x}M_x)_3O_7$ (M=Co, Zn; $0 \leq x < 0.1$) (YBCO-$x\%M$) were made by a standard solid state reaction method. Details of sample preparation and characterization are given in Ref. 2. Bar-shape samples, $1 \times 1 \times 10$ mm^3, were cut off from sintered bulk samples for measuring the inter- and intragrain critical-current

densities $J_{c(\text{inter})}$ and $J_{c(\text{intra})}$. They were reannealed in oxygen at 420 °C for 12 h to recover the possible oxygen loss during the cutting. On the other hand, in order to obtain single-crystalline oriented samples, the samples were ground into fine powders and magnetically aligned in wax at room temperature in a field of 6 T.[2] To calculate the penetration depth from ac susceptibility data, the grain size distribution was measured using scanning electron microscopy (SEM) for four samples, $YBa_2Cu_3O_7$ (YBCO), $YBa_2(Cu_{0.985}Co_{0.015})_3O_7$ (YBCO-1.5%Co), $YBa_2(Cu_{0.96}Co_{0.04})_3O_7$ (YBCO-4%Co), and $YBa_2(Cu_{0.95}Zn_{0.05})_3O_7$ (YBCO-5%Zn). A commercial (Lake Shore ac susceptometer 7000), a laboratory-made ac susceptometer,[16] and a vibrating sample magnetometer (VSM 3001, Oxford Instrument) were used to measure ac susceptibility, intergrain critical-current density $J_{c(\text{inter})}$, upper critical field H_{c2}, magnetization M, intragrain critical current density $J_{c(\text{intra})}$, and the irreversibility line.

An ac inductive technique[17-19] was used to measure $J_{c(\text{inter})}$ of the samples. A drive coil provided a sinusoidal field at 800 Hz whose amplitude could be varied up to 20 mT. A search coil around the sample measured the flux entering it. The derivative of the signal s with respect to the amplitude b_0 is a measure of the depth to which currents flow and a marked discontinuity is seen when the flux reaches the sample center. If the amplitude of the applied field at this point is b_0^* then according to the Beam model $J_{c(\text{inter})} = b_0^* / a_1\mu_0$, where $2a_1$ is the sample thickness.

The upper critical field H_{c2} was determined directly near T_c from $M(T)$ curves of the aligned samples measured at fixed fields. The irreversibility line $H_{\text{irr}}(T)$ is determined as the onset of detectable irreversibility in the isothermal dc M-H loops. Certainly, the value of H_{irr} depends on the sensitivity and the noise level of the instrument and a criterion 10^{-5} emu (that is the noise level of the VSM) was used. It corresponds to a J_c value of 100 A/cm^2. By using the same criterion for all samples, it is possible to draw conclusions on the effect of doping, even if the absolute value is uncertain. $J_{c(\text{intra})}$ was calculated from magnetic hysteresis using the Bean model.

III. RESULTS AND DISCUSSION

A. ac susceptibility (χ) and penetration depth (λ)

In Fig. 1, we show the ac susceptibility (χ) data of three samples (YBCO, YBCO-4%Co, and YBCO-5%Zn). The data were normalized with respect to full diamagnetic susceptibility (χ_{max}) which was calculated from the volume of the superconducting materials contained in the aligned samples.[2] The data show clearly the expected reduction in the diamagnetic susceptibility due to the field penetration into the superconducting grains. Evident difference in susceptibilities for the field parallel to the c-axis (χ_c) and ab plane (χ_{ab}) reflects the anisotropic nature of high-T_c superconductors due to the layered structure. With increasing the doping concentration, both χ_{ab} and χ_c are decreased, indicating larger penetration depths in the doped material. The increase in λ is
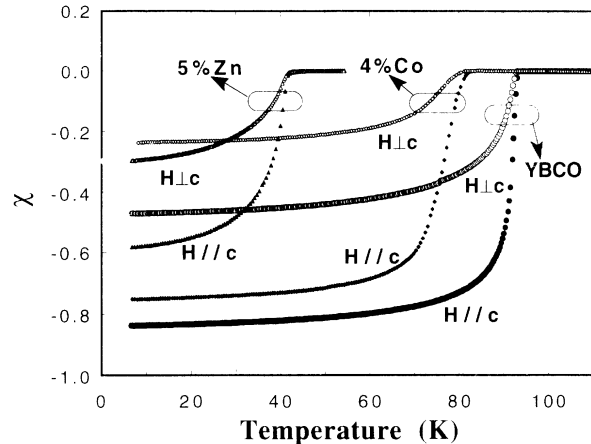
FIG. 1. The temperature dependence of the ac susceptibility χ of magnetically aligned powders of YBCO, YBCO-4%Co, and YBCO-5%Zn with the field parallel ($H\|c$) and perpendicular ($H\perp c$) to the c axis.

probably largely caused by a decrease of superconducting pair density n_s. According to the London theory, λ is related to n_s by

$$\lambda^2 = \frac{m^*}{\mu_0 n_s e^2} \, , \tag{1}$$

where m^* is the effective mass of the electron. The progressive decrease of n_s has also been observed in specific heat[3,4] and possibly in Hall effect measurements.[20] Finally, when plotting χ_c/χ_{ab} at low temperatures (~ 4.2 K) as a function of the doping concentration, as shown in Fig. 2, we find that for the Co-doped YBCO χ_c/χ_{ab} increases much more rapidly than the Zn-doped YBCO. We attribute the large variation of χ_c/χ_{ab} in Co-doped
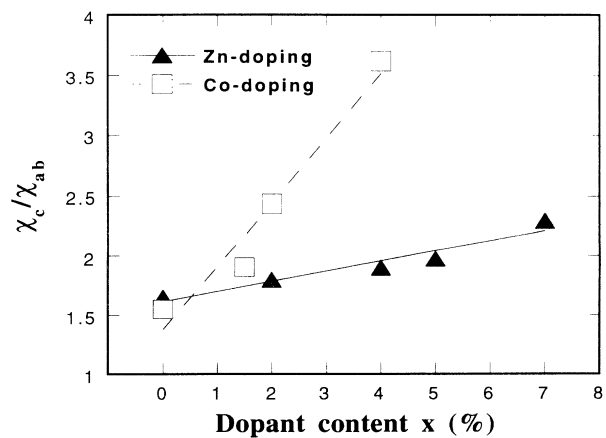
FIG. 2. The ratio of χ_c/χ_{ab} (χ_c, χ_{ab}, ac susceptibility with field parallel to the c axis and ab plane, respectively) as a function of doping content for the Co- and Zn-doped YBCO samples.

samples to increasing anisotropy with Co concentration, i.e., an increase in m^* for the c direction. This can be understood qualitatively in terms of different substitution sites of Co and Zn dopants. In YBCO and all high-T_c superconductors, the superconductivity is associated with the CuO_2 planes and the conducting CuO chains in YBCO improve the interplanar coupling between superconducting planes. The substitution of Co for Cu in the chain site reduces the coupling and therefore increases the anisotropy. In contrast, Zn dopants go into the CuO_2 plane and thus have little effect on the anisotropy. The increased anisotropy leading to larger fluctuations effects are also observed in the conductivity[21] above T_c and in the magnetization of Co-doped YBCO.

Assuming the superconducting grains in the composite samples are spherical, values of penetration depth for the YBCO, YBCO-1.5%Co, YBCO-4%Co, and YBCO-5%Zn samples were calculated from the ac susceptibility data χ/χ_{max} shown in Fig. 1 using the formula[22]

$$\frac{\chi}{\chi_{max}} = 1 - 3x \coth\left[\frac{1}{x}\right] + 3x^2 , \tag{2}$$

where $x = \lambda/a$. (a is the radius of a grain.) The details of the calculation and the temperature dependence of λ_{ab} and λ_c have been reported previously.[2] The low-temperature values are listed in Table I. For the pure YBCO sample, values of both λ_{ab} and λ_c are in good agreement with the values reported in literature.[23–27]

B. Coherence length (ξ), lower and upper critical fields (H_{c1} and H_{c2}), and Ginzburg-Landau parameter (κ)

For an anisotropic superconductor, a reduced effective-mass tensor is introduced to account for anisotropic properties. The tensor is diagonal, its elements m_i are normalized by $m_1 m_2 m_3 = 1$. The characteristic lengths ξ and λ along the principal axes are determined by $\xi_i = \xi/\sqrt{m_i}$ and $\lambda_i = \lambda\sqrt{m_i}$, where $\xi = (\xi_1\xi_2\xi_3)^{1/3}$ and $\lambda = (\lambda_1\lambda_2\lambda_3)^{1/3}$. The high-$T_c$ superconductors are usually regarded as uniaxial superconductors, i.e., their anisotropy between a-axis and b-axis directions is neglected, and hence $\xi_a = \xi_b = \xi_{ab}$ and $\lambda_a = \lambda_b = \lambda_{ab}$. In this case ξ, λ, and κ are related to critical fields through following relations:

$$H_{c1}^c = \frac{\phi_0}{4\pi\lambda_{ab}^2}(\ln\kappa_c + 0.5) ,$$

$$H_{c1}^{ab} = \frac{\phi_0}{4\pi\lambda_{ab}\lambda_c}(\ln\kappa_{ab} + 0.5) , \tag{3}$$

$$H_{c2}^c = \frac{\phi_0}{2\pi\xi_{ab}^2} , \quad H_{c2}^{ab} = \frac{\phi_0}{2\pi\xi_{ab}\xi_c} , \tag{4}$$

$$H_c = \frac{\phi_0}{2\sqrt{2}\pi\xi_{ab}\lambda_{ab}} , \quad H_c = \frac{\phi_0}{2\sqrt{2}\pi\xi_c\lambda_c} , \tag{5}$$

where

$$\kappa_c = \lambda_{ab}/\xi_{ab}$$

and   (6)

$$\kappa_{ab} = \lambda_c/\xi_{ab} = [(\lambda_c/\xi_c)(\lambda_{ab}/\xi_{ab})]^{1/2} .$$

The penetration depth and the coherence length are related to the mass anisotropy by

$$\lambda_c/\lambda_{ab} = \xi_{ab}/\xi_c = (m_c/m_{ab})^{1/2} . \tag{7}$$

It is worth pointing out that the thermodynamic critical field H_c is isotropic. This is because $\frac{1}{2}\mu_0 H_c^2$ is the condensation energy per unit volume of a superconductor, and hence is independent of external fields or their direction.

The thermodynamic critical field $H_c(T)$ of these four samples were obtained by Loram et al.[3,4] from the specific-heat data. The specific-heat measurements were carried out on another batch of the original samples from which the aligned composite samples were made. By employing a differential technique, the large contribution of phonons to the specific heat can be backed off, and hence a high resolution of 0.01% can be achieved. This permits the electronic specific heat, which is most relevant to the superconductivity, to be measured accurately. From these measurements, the difference of the electronic specific heat between the superconducting state and the normal state ΔC^{el} is obtained. Then the entropy difference can be calculated as

$$S_s(T) - S_n(T) = \int_{T_c}^{T} \frac{\Delta C^{el}(T')}{T'} dT' . \tag{8}$$

Thus, $H_c(T)$ is calculated by the relation

TABLE I. Penetration depth, coherence length, critical fields, and Ginzburg-Landau parameter of magnetically aligned $YBa_2(Cu_{1-x}M_x)_3O_7$ (M = Co,Zn). λ_{ab} and λ_c were obtained from the ac susceptibility data (Ref. 2). The data of H_c were obtained from a specific-heat measurement (Refs. 3 and 4). Other parameters are calculated using the Ginzburg-Landau relations (see text).

	λ_{ab} (nm)	λ_c (nm)	H_c (T)	κ_{ab}	κ_c	ξ_{ab} (nm)	ξ_c (nm)	H_{c1}^{ab} (mT)	H_{c1}^c (mT)	H_{c2}^{ab} (T)	H_{c2}^c (T)
Pure YBCO	135	894	1.1	85	560	1.6	0.24	8.9	50	850	130
1.5% Co	190	998	0.84	130	680	1.5	0.28	6.3	30	800	150
4% Co	188	1717	0.43	65	590	2.9	0.32	3.3	25	360	40
5% Zn	312	1301	0.24	100	420	3.1	0.74	2.6	9.4	140	34

$$\frac{\mu_0 H_c^2(T)}{2} = f_n(T) - f_s(T)$$

$$= \int_{T_c}^{T} [S_s(T') - S_n(T')]dT \ , \tag{9}$$

where f_n and f_s are the free-energy densities of the normal state and superconducting state.

From λ and H_c the other parameters were calculated using Eqs. (3)–(6). The zero-temperature results are listed in Table I. For pure YBCO results are in agreement with those reported in the literature. For example, the value of H_{c2}^c is in good agreement with that obtained by Welp et al.[28] on single crystals. The values of H_{c2}^{ab} seems slightly larger than theirs, and consequently gives a slightly higher anisotropy of 6.3 compared with 5.2 in their paper. However, this value of anisotropy is consistent with results from torque magnetometery[29] and another report.[30] As shown in Table I, the data indicate that Co doping increases the anisotropy [as reflected by $\lambda_c(0)/\lambda_{ab}(0)$ or $\xi_{ab}(0)/\xi_c(0)$], while the increase in $\lambda_{ab}(0)$ is just in excess of the experimental uncertainty. In contrast, Zn doping gives a particularly strong increase in $\lambda_{ab}(0)$. It is tempting to associate this difference between Co and Zn doping to their different substitution sites in the YBCO crystal unit cell. The chain site substitution of Co may reduce the coupling between the superconducting CuO_2 plane and therefore increases the anisotropy. The increase of the anisotropy in the Co-doped sample is consistent with the larger fluctuation effects observed in the conductivity above T_c.[21]

It is also interesting to notice that for the doped samples the coherence length ξ increases and the Ginzburg-Landau parameter κ does not change much. This seems different from the doping effect in log-T_c metals. For a low-T_c superconductor, the presence of impurities reduces the mean-free-path l and hence the coherence length ξ decreases according to the relation[31]

$$\frac{1}{\xi} = \frac{1}{\xi_0} + \frac{1}{l} \ . \tag{10}$$

Here ξ_0 is the BCS coherence length for pure metals and is related to the superconducting transition temperature T_c and Fermi velocity V_F by the relation[32]

$$\xi_0 = 0.15 \frac{\hbar V_F}{k_B T_c} \ . \tag{11}$$

However, for high-T_c superconductors, ξ_0 is very short compared with l even in doped samples. Therefore, they remain in the clean limit, $\xi_0 \ll l$, and so ξ is mainly determined by ξ_0. Both T_c and V_F (which is a function of n_s and m^*) decrease with doping, as indicated by susceptibility and the penetration depth data. If the reduction of T_c by doping is greater than that of V_F, according to Eq. (11) the coherence length could increase.

The temperature dependences of H_{c1} and H_{c2} of pure YBCO and the YBCO-5%Zn sample, obtained from Eqs. (3)–(5) and the measured values of $H_c(T)$ and $\lambda(T)$, are shown in Fig. 3. The discontinuity near T_c in the H_{c2} diagram is due to fluctuation effects in $H_c(T)$ and it is not clear how they should be smoothed out in calculating

H_{c2}. Apart from this, the overall temperature dependence of H_{c1} and H_{c2} is similar to that of a conventional superconductor. In the literature there are reports that the temperature dependence of H_{c1} shows an unusual upturn rather than a saturation at low temperatures.[33–38] This unusual temperature dependence is in contradiction with the Ginzburg-Landau theory and the data presented here. Some sophisticated models including the model of a layered superconductor coupled via proximity effect[39] and the two superconducting phase models[40] have been proposed to explain this upturn. However, since this kind of unusual temperature dependence of H_{c1} was usually presented in experiments using magnetization measurements to determine H_{c1}, it is probable that the upturn resulted from surface or bulk pinning. In the magnetization measurement, H_{c1} is defined as the field at which the magnetization M starts to deviate from linearity. However, the strong pinning prevents flux moving inside the sample at low field and leads to an apparently linear behavior in the M-H curve to fields higher than H_{c1}. Hence H_{c1} determined in this way is often higher than the real value and follows the temperature dependence of the pinning force or the critical current which
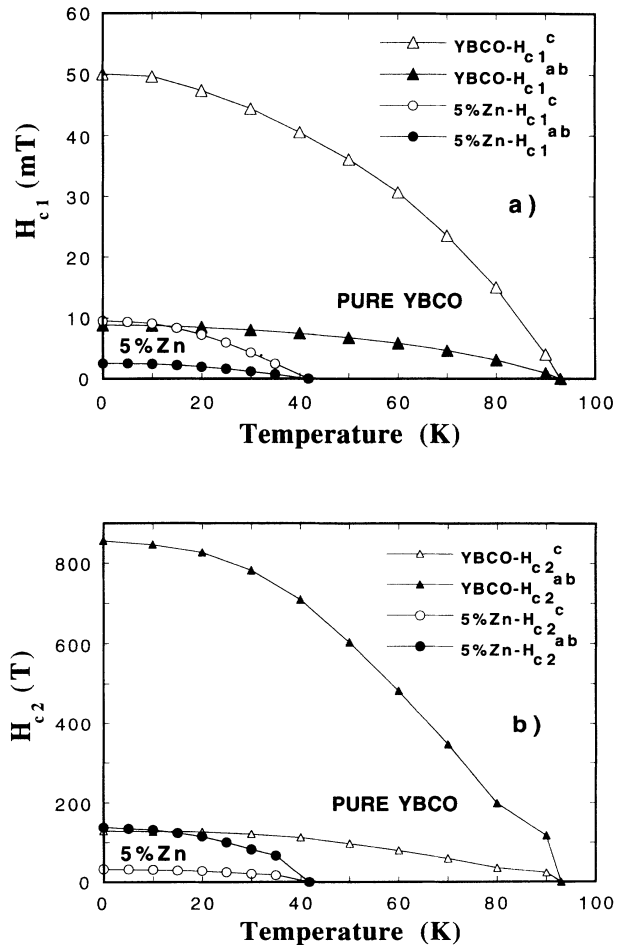
FIG. 3. The temperature dependence of (a) H_{c1} and (b) H_{c2} for the YBCO and YBCO-5%Zn samples. H_{c1} and H_{c2} were calculated from λ and H_c using Eqs. (3)–(5) (see text).

does not saturate at low temperatures. Naito et $al.$[41] have shown that H_{c1} can be measured more properly if the pinning effect can be accounted for by analyzing magnetization data with the Bean model. The H_{c1} results presented here were extracted from the penetration depth, and thus do not show the upturn behavior.

The temperature dependence of $H_{c2}(T)$ is an important clue to understand the pairing mechanism of high-T_c superconductors. The BCS theory gives a linear relation at temperatures near T_c, while some other theoretical models give a different temperature dependence. According to the bipolaron superconductivity mechanism, for example, H_{c2} follows a relation $(1-T/T_c)^{3/2}$ which means a positive curvature.[42] Although the uncertainty of H_{c2} near T_c makes the verification of the relation difficult, the overall behavior of measured $H_{c2}(T)$ seems more in agreement with the traditional theory.

C. Direct measurement of the upper critical field H_{c2}

In order to check the results in Table I independently, we measured the upper critical field H_{c2} of these samples with the field parallel to the c axis. The measurements were performed in the VSM with fields up to 6 T. It is observed that in a temperature interval of about 10 K (depending on the applied field) below T_c the magnetization is reversible. Therefore, these measurements reflect an equilibrium state and are not complicated by effects due to pinning. In Fig. 4, the zero-field-cooled (ZFC) magnetization curves are shown as a function of temperature and applied field oriented parallel to the c axis for the YBCO sample. A linear temperature dependence of the magnetization below T_c is clearly shown. The nucleation temperature $T_{c2}(H)$ is defined as the intercept of a linear extrapolation of the magnetization in the superconducting state with the normal-state base line. The data display nicely the depression of T_c with field. In the near vicinity of the transition, rounding in the $M(T)$ dependence is shown. This broadening is probably caused by diamagnetic fluctuations. For the YBCO-5%Zn sample and the YBCO-1.5%Co sample, a similar
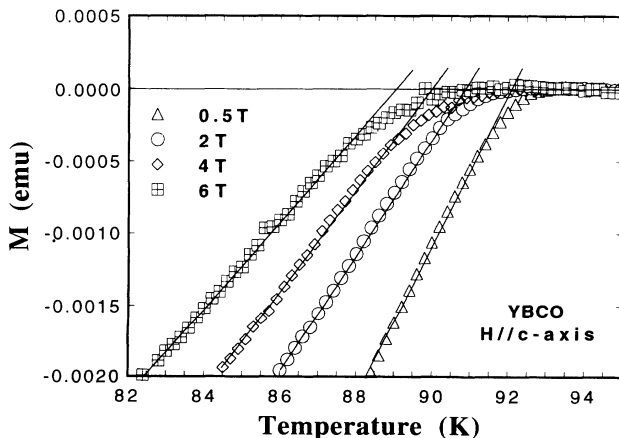
temperature dependence to that shown in Fig. 4 was also obtained. However, for the YBCO-4% Co sample the transition is very broad and there is no well-defined onset temperature $T_{c2}(H)$. This is attributed mainly to the enhanced fluctuation effects due to the increase of the anisotropy. Microwave[21] and resistivity measurements[43] have shown that in the Co-doped-YBCO samples the fluctuation effect is indeed larger at high concentrations. For the orientation of the applied field parallel to the ab plane, the slope dH_{c2}/dT is too large so that with our experimental resolution the depression of T_c by field cannot be seen clearly.

In Fig. 5, H_{c2} is plotted as a function of temperature at temperatures near T_c for the YBCO and YBCO-5%Zn samples. A linear dependence fits the data well for both samples. Data for YBCO-1.5%Co are not shown on the graph, but follow the same linear temperature dependence as the other two. The critical-field slopes from the linear fits are -2.01, -2.32, and -1.45 T/K for the YBCO, YBCO-1.5%Co, and YBCO-5%Zn samples, respectively. Correspondingly, the upper critical field extrapolated to $T=0$ using the relation[44]

$$H_{c2}(0)=0.7T_c(\partial H_{c2}/\partial T)|_{T_c} \qquad (12)$$

and the coherence lengths calculated using Eq. (6) are $H_{c2}^c(0)=129$, 152, and 41 T and $\xi_{ab}(0)=1.57$, 1.47, and 2.83 Å for these three samples. Comparing this to the data in Table I, the results of YBCO and YBCO-1.5%Co are in good agreement with that obtained in the previous section. For YBCO-5%Zn, the direct measurement yields a higher value of H_{c2} than does the method described in Sec. III E, but is reasonably consistent.

The experimental data in Fig. 5 appear to show a linear temperature dependence, consistent with the Ginzburg-Landau theory. However, taking into account of the experimental error and the narrow temperature region over which the data are obtained, the possibility of other temperature relations, for instance, the $(1-T/T_c)^{3/2}$ dependence suggested in the bipolaron boson model, cannot be ruled out entirely.

FIG. 4. Zero-field-cooled magnetizations measured at different fields as a function of temperature for the YBCO sample.
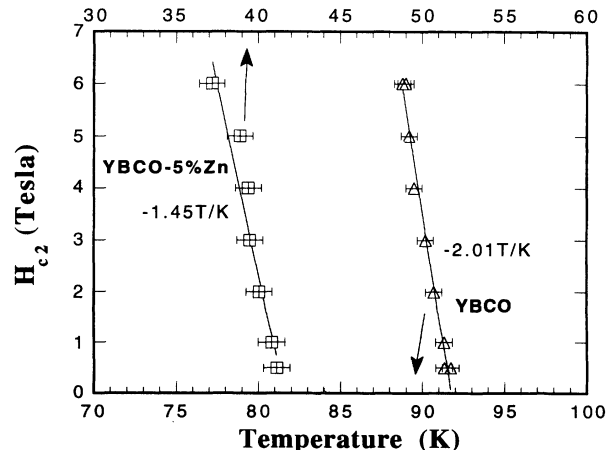
FIG. 5. High-temperature values of H_{c2} near T_c, measured from the magnetization, of the YBCO and the YBCO-5%Zn sample.

D. Inter- and intragrain critical currents

($J_{c(\text{inter})}$ and $J_{c(\text{intra})}$)

The intergrain critical current of Co and Zn-doped samples was measured using a inductive method[17-19] on bar-shaped samples cut off from the original sintered samples. The sample was cooled down to 4.2 or 77 K in zero field, and then temperature became stable a small ac field ($b = b_0 \cos\omega t$) was applied for balancing the output and adjusting the phase of the lock-in amplifier. The phase was set to give a maximum signal and the balance was made by adjusting the compensating coil to give a zero output. After doing this, the ac applied field was sweeping up slowly while V, the voltage output of the lock-in amplifier, was recorded. The derivative $\partial V/\partial b_0$ was computed numerically afterwards.

The inductive method employed here measures the total flux put into the sample by the applied ac field. As pointed out previously,[17,19] the plot of b versus $\partial V/\partial b_0$ reflects the magnetic flux profile inside the sample. In the case of a long slab and within the Bean model ($J_c = $const), this is straightforward. In the case of the Anderson-Kim model ($J_c \propto 1/H$), the derivative gives J_c as a function of b_0, but again it also gives the penetration for a value of J_c averaged over the amplitude b_0. If the sample is cylindrical or rectangular, its surface shell can be regarded as a slab and hence the above discussion still holds for small field amplitudes when flux penetrates only into the edge area. For a large field amplitude where the flux penetration goes to the center of the sample, J_c can be calculated as an average over b_0. In Fig. 6, some calculated b_0 against $\partial V/\partial b_0$ curves for different sample geometries and $J_c(B)$ dependence are presented. The sample is a long rectangular rod with cross section $2a_1 \times 2a_2$. A notable point is that if the results are analyzed using the Anderson-Kim model ($J_c \propto 1/B$) a curvature is shown at low fields and a peak is shown near the full penetration field b_0^* (the field at which flux lines reach the center of the sample). The peak position, as shown in Fig. 6(b), does not always coincide with b_0^* but varies slightly with the sample geometry.

A sintered bulk sample can be regarded as a network of superconducting grains connected by weak links.[45,46] In the inductive technique, the applied field is small so that it penetrates into the sample mainly through the weak links at grain boundaries. Thus, the critical-current density measured here is $J_{c(\text{inter})}$.

Some raw data for three samples recorded at 4.2 K and their derivative are shown in Figs. 7(a) and 7(b), respectively. The curvature at low fields and the peak at higher fields are seen clearly in the field b_0 against the derivative $\partial V/\partial b_0$ plot [Fig. 7(b)] for these three samples. The similarity between the measured curves and those shown in Fig. 6(b) shows clearly a strongly field dependent $J_{c(\text{inter})}$ as we expected for a sintered bulk samples. The average value of $J_{c(\text{inter})}$ is determined by $b_0^* /(\mu_0 a_1)$, where b_0^* is the peak field and $2a_1 (=1$ mm) is the sample thickness. For the pure YBCO sample, $J_{c(\text{inter})}$ is about 100 A/cm^2 which is 3 or 4 orders of magnitude lower than $J_{c(\text{inter})}$, the critical-current density within grains. With the addition of more Co or Zn, $J_{c(\text{inter})}$ decreases.

dc magnetization measurements were also performed on the samples used in the ac inductive measurements in an applied field of up to 12 T. It is believed that at sufficiently high field, for instance, 1 T, the weak links at grain boundaries become nonsuperconducting so that the contribution of $J_{c(\text{inter})}$ to magnetization is unimportant. In this case, according to the Bean model,[47] we have $J_{c(\text{intra})} \propto \Delta M /d$, d is the particle size, where ΔM is the magnetic hysteresis of increasing and decreasing field. Therefore, the change of ΔM mirrors the change of $J_{c(\text{intra})}$ (the samples were made under same conditions, and thus d has a similar value). For the pure YBCO sample, using the grain size $d = 2$ μm and the formula derived from the Bean model,[47]

$$J_{c(\text{intra})} = 34\Delta M /d \tag{13}$$

(J_c, A/cm^2; ΔM, emu/cm^3; d, cm), we obtain a value of 1.7×10^7 A/cm^2 that is much higher than $J_{c(\text{inter})}$.

In Figs. 8(a) and 8(b), we show the inter- and intragrain critical currents as a function of doping concentration for the Co- and Zn-doped samples, respectively. Values of
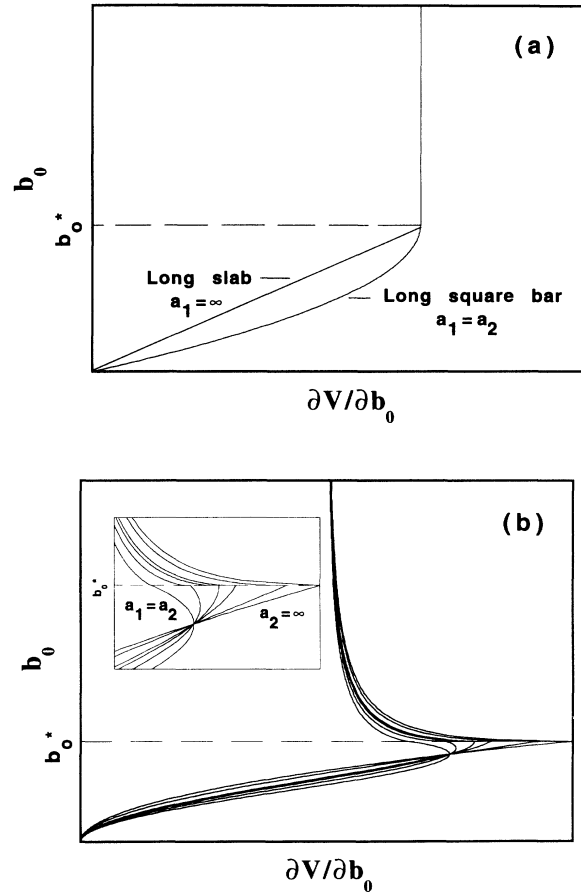
FIG. 6. Calculated b_0 against $\partial V/\partial b_0$ (b_0 is the amplitude of the ac field and V is the output of the lock-in amplifier) curves according to (a) the Bean model $J_c =$const and (b) the Anderson-Kim model $J_c \propto 1/B$. The sample is a long rectangular rod with cross section $2a_1 \times 2a_2$. The inset in (b) shows the detail around the peak.

$J_{c(\text{inter})}$ and $J_{c(\text{intra})}$ are normalized to the value of the un-doped sample. It is clear that both $J_{c(\text{inter})}$ and $J_{c(\text{intra})}$ decrease with increasing the doping concentration. Furthermore, the two critical currents show a very similar decay rate with doping concentration, although there is inevitably a good deal of scatter in the experimental data and the absolute magnitudes differ by a factor 10^3. The results suggest that $J_{c(\text{inter})}$ scales with $J_{c(\text{intra})}$, which is at first sight surprising since it is usually assumed that the limited mechanisms are quite different. On close examination the result is consistent with a number of pictures. First, if the boundaries are SIS (superconductor-insulator-superconductor) type and the thickness does not change, $J_{c(\text{inter})}$ will vary with the energy gap and it is likely that bulk pinning energies will vary in a similar way. Second, if the boundaries are SNS (superconductor-normal-superconductor) type, J_c will be determined by the order parameter on either side of the boundary and the coherence length within the boundary.

If the dopants do not affect the nature of the grain boundary layer significantly we would again find scaling of the two current densities. Thus, our results suggest that doping does not affect significantly the width or properties of the boundary between grains.

Additionally dc magnetization measurements have been undertaken on the magnetically aligned composites. In this case no intergrain currents are involved at all. Results measured at 4.2 K with field parallel to the c axis are shown in Fig. 9. All curves show a similar field dependence, with almost field-independent magnetization at high fields indicating a high and field-independent $J_{c(\text{intra})}$. The smaller size of the hysteresis means that $J_{c(\text{inter})}$ decreases as Cu is partially substituted.

To correlate $J_{c(\text{intra})}$ with the superconducting parameters, we consider a simplified single-site pinning model. In this model, the pinning force density $F_p = J_c B$ (where B is the flux density) can be linked to the pinning energy (related to the condensation energy) and the coherence
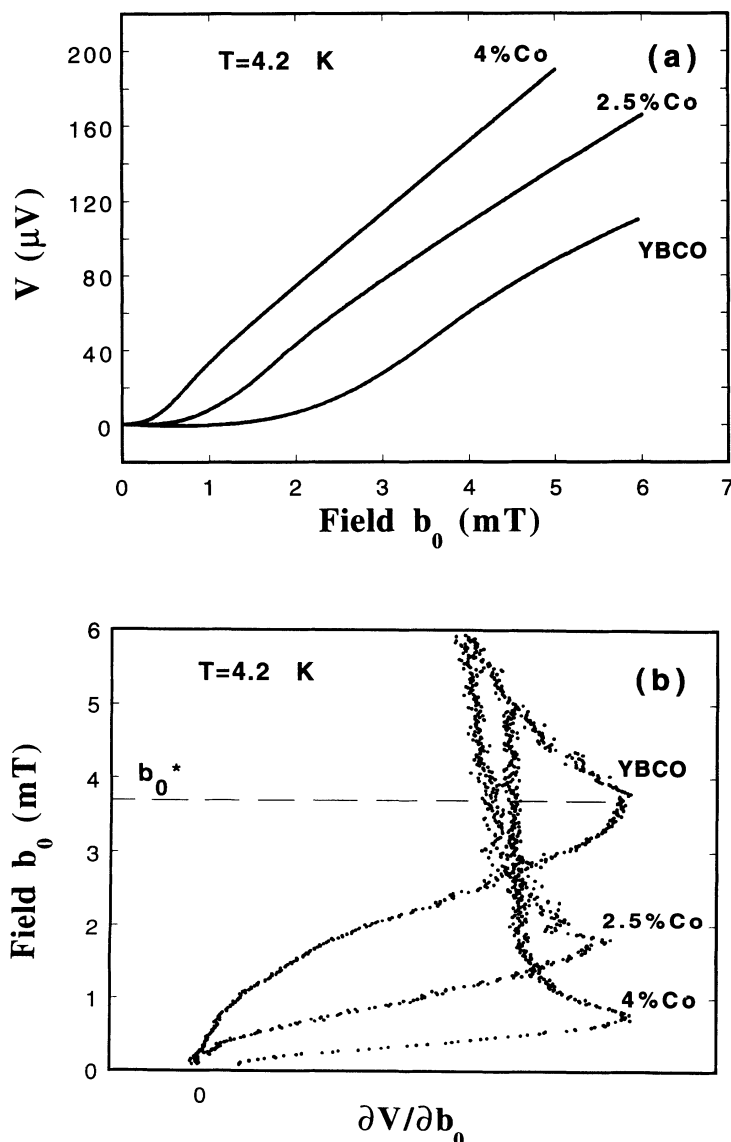
FIG. 7. Experimental data of (a) V vs b_0 and (b) b_0 vs $\partial V / \partial b_0$ for Co-doped YBCO bulk samples. The data in (b) were calculated numerically from those in (a). Similarity of curves in (b) with those in Fig. 6(b) suggests $J_{c(\text{inter})}$ is strongly field dependent. The average $J_{c(\text{inter})}$ over b_0^* (the peak field) is determined as $J_{c(\text{inter})} = b_0^* / (\mu_0 a_1)$.
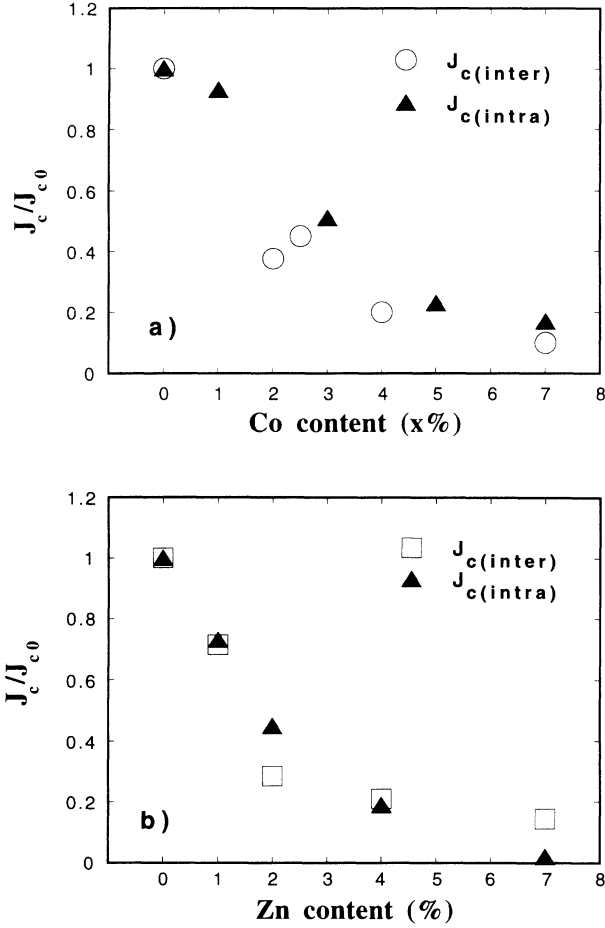
FIG. 8. Critical-current densities of (a) the Co-doped samples and (b) the Zn-doped samples measured at 4.2 K with using ac inductive technique (for $J_{c(\text{inter})}$) and dc magnetization (for $J_{c(\text{intra})}$). Results of both $J_{c(\text{inter})}$ and $J_{c(\text{intra})}$ are normalized by values of the pure YBCO sample.
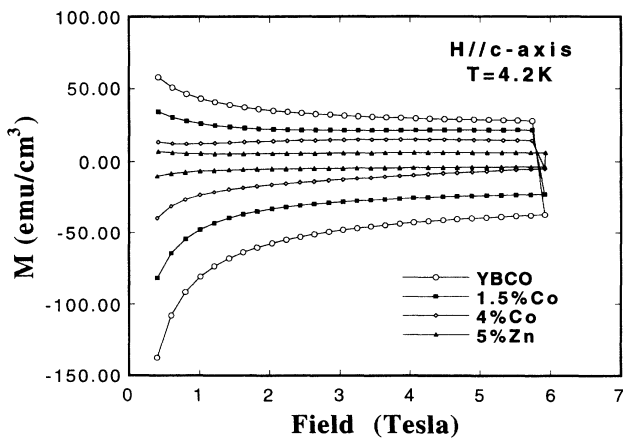
length in a straightforward manner. Consider the situation of field parallel to the c axis. The energy of the core of a vortex is $E = \frac{1}{2}\mu_0 H_c^2 \xi_{ab}^2$ per unit length so the maximum force in creating a core is $\nabla E \approx \frac{1}{2}\mu_0 H_c^2 \xi_{ab}$. This is the pinning force. The driving force (Lorentz force) per line is $\phi_0 J_c$ per unit length so that we can write $J_{c(\text{intra})}$ as

$$J_{c(\text{intra})} = \eta \mu_0 H_c^2 \xi_{ab} / 2\phi_0 , \qquad (14)$$

where η is a numerical factor accounting for incomplete suppression of the order parameter at the pinning site and other deviations from the optimal case. In a real system, the situation is expected to be more complex. However, the essential characteristics of flux pinning are contained in this simplified form. According to Eq. (14), a linear relation between J_c and the product $\mu_0 H_c^2 \xi_{ab}$ is expected. In Fig. 10, $J_{c(\text{intra})}$ of four samples (YBCO, YBCO-1.5%Co, YBCO-4%Co, and YBCO-5%Zn) measured at 4.2 K and 1 T with the field parallel to the c axis is shown as a function of $\mu_0 H_c^2(0)\xi_{ab}(0)/2$ (H_c and ξ_{ab} values are from Table I) for corresponding samples. The graph shows a reasonable proportionality between the two quantities, supporting the essential validity of the above simple single-site pinning model for predicting the effect of doping. Also the result shown in Fig. 10 suggests that the strength of the pinning in high-T_c superconductors is strongly influenced by the thermodynamic properties such as H_c and ξ, and thus any attempts to introduce pinning centers have to be done without lowering the value of H_c. In this regard, point or columnar defects produced by neutron,[48] proton,[49] and heavy-ion[50] irradiation and small precipitates of Y_2BaCuO_5 in $YBa_2Cu_3O_7$ (Ref. 51) may act as such candidates. Additionally, using Eq. (5), J_c can be written as

$$J_c \propto H_c^2 \xi_{ab} \propto H_c / \lambda_{ab} , \qquad (15)$$

that is the depairing current. Therefore, $J_{c(\text{intra})}$ scales with the depairing current. Also, Eq. (15) suggests that for the purpose of applications we should look for materials with small λ (or high H_{c1})

FIG. 9. Magnetic hysteresis loops of the magnetically aligned YBCO, YBCO-1.5%Co, YBCO-4%Co, and YBCO-5%Zn samples with field parallel to the c axis.
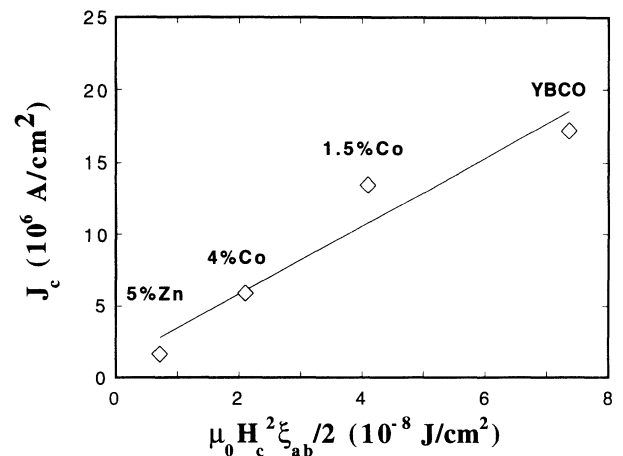
FIG. 10. The intragrain critical current density $J_{c(\text{intra})}$ at 4.2 K and 1 T shown as a function of the product $\mu_0 H_c^2 \xi_{ab}$.

E. The irreversibility line

In Fig. 11, we show the irreversibility line $H_{irr}(T)$ of the YBCO, YBCO-1.5%Co, YBCO-4%Co, and YBCO-5%Zn samples. Because H_{c2} and T_c change with Co and Zn substitution, all fields and temperatures in this diagram are normalized to $H_{c2}(0)$ and T_c of the corresponding sample, respectively. The H_{c2} values of YBCO, YBCO-1.5%Co, and YBCO-5%Zn are those measured experimentally as described in Sec. III D. For the YBCO-4%Co sample, H_{c2} could not be measured directly, and hence the value listed in Table I is used. It is noteworthy that the normalized irreversibility line of the Zn-doped sample seems identical to that of the undoped sample. At lower temperatures or high fields, the irreversibility of the two samples may become quite different, but at least below $0.3H_{c2}$ the magnetic phase diagram seems to be unchanged by the Zn doping even although T_c is reduced drastically. However the effect of Co doping seems different, the irreversibility line is more curved and eventually is pushed to much lower temperature or field with increasing the Co dopant. The magnetic reversible region expands rapidly with doping.

We have seen in Secs. III A and III B that Co doping results in a large increase in anisotropy. Thus, the results presented here strongly suggest that in high-T_c superconducting oxides the degree of their anisotropic character is a key factor in determining the irreversibility line. In high-T_c superconductors, due to their layered structure, flux lines along the c axis might be regarded as vortex pancakes[52] coupled via the Josephson effect and their magnetic interaction. In YBCO, CuO chains, which are believed to be conducting, are present between superconducting CuO_2 biplanes, and hence enhance the coupling along the c axis, resulting in a good flux pinning and critical-current behavior at high temperatures and high fields, and a high irreversibility line compared to other high-T_c superconductors. When Co ions are doped into the CuO chains, they presumably weaken the coupling and cause the vortex lattice to more easily break into pancakes which are easily thermally activated, leading to a low irreversibility line.[53,54]

IV. SUMMARY

In summary, the effect of Co and Zn doping on the superconducting properties of YBCO has been studied by means of ac susceptibility and dc magnetization. By using magnetically aligned powdered samples, the magnetic penetration depth λ_{ab} and λ_c could be measured. Both λ_{ab} and λ_c were decreased by doping. However, the effects of Co and Zn doping on the anisotropy of YBCO are different. The experimental data indicate that Co doping increases the anisotropy [as reflected by $\lambda_c(0)/\lambda_{ab}(0)$ or $\xi_{ab}(0)/\xi_c(0)$], while the increase in
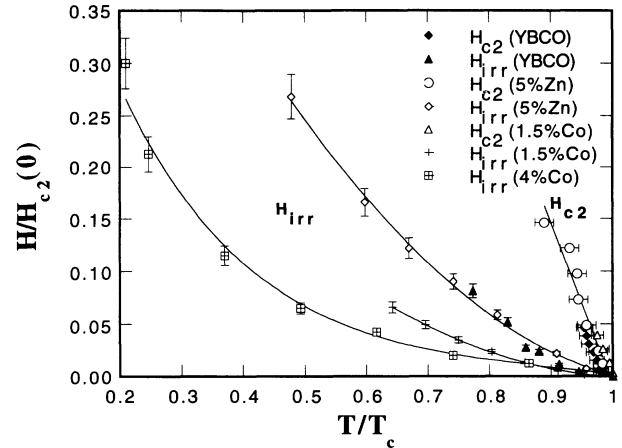
FIG. 11. The irreversibility line and upper critical field (H_{c2}) of YBCO, YBCO-1.5%Co, YBCO-4%Co, and YBCO-5%Zn. The fields and temperatures are normalized to $H_{c2}(0)$ and T_c, respectively.

$\lambda_{ab}(0)$ is just in excess of the experimental uncertainty. In contrast, Zn doping gives a particularly strong increase in $\lambda_{ab}(0)$. This can be understood by linking the anisotropy difference between Co and Zn doping to their different substitution sites in the YBCO crystal unit cell. The chain site substitution of Co probably reduces the coupling between the superconducting CuO_2 plane and therefore increases the anisotropy. With the aid of the Ginzburg-Landau relations, basic superconducting parameters such as the upper and lower critical fields, H_{c1} and H_{c2}, the coherence length ξ, and the Ginzburg-Landau parameter κ were calculated from λ and the thermodynamic critical field H_c, which was determined from specific-heat measurements. The values of H_{c2} measured directly near T_c were consistent with these estimated values. Both inter- and intragrain critical-current densities, $J_{c(inter)}$ and $J_{c(intra)}$, decreased with doping. $J_{c(intra)}$ showed good correlation with the pinning model parameter $\frac{1}{2}\mu_0 H_c^2 \xi_{ab}$. This suggested that the decrease the condensation energy $\frac{1}{2}\mu_0 H_c^2$ by doping is responsible for the reduction of J_c. Moreover, the irreversibility line was lowered by doping, in particular by Co doping which weakens the interlayer coupling and increases the anisotropy. The results strongly indicated that in high-T_c superconducting oxides the degree of their coupling between planes is a key factor in determining the irreversibility line.

*Present address: School of Electronic and Electrical Engineering, University of Birmingham, Birmingham, B15 2TT, United Kingdom.

[1]A. M. Campbell and J. E. Evetts, Adv. Phys. **21**, 199 (1972).

[2]A. Porch, J. R. Cooper, D. N. Zheng, J. R. Waldram, A. M. Campbell, and P. A. Freeman, Physica C **214**, 350 (1993).

[3]J. W. Loram, K. A. Mirza, and P. A. Freeman, Physica C **171**, 243 (1990).

[4]J. W. Loram, K. A. Mirza, P. M. Freeman, and J. J. Tallon, Supercond. Sci. Technol. **4**, S184 (1991).

[5]K. Maki, Physics **1**, 127 (1964).

[6]G. Eilenberger, Phys. Rev. **153**, 584 (1967).

[7]V. J. Emery, Phys. Rev. Lett. **58**, 2794 (1987).

[8]A. W. Sleight, Science **242**, 1519 (1988).

[9]R. J. Cava, Science **247**, 656 (1990).

[10]G. Xiao, M. Z. Cieplak, A. Gavrin, F. H. Streitz, A. Bakhshai, and C. L. Chien, Phys. Rev. Lett. **60**, 1446 (1988).

[11]J. M. Tarascon, P. Barboux, P. F. Miceli, L. H. Greene, and G. W. Hull, Phys. Rev. B **37**, 7458 (1988).

[12]G. Xiao, M. Z. Cieplak, D. Musser, A. Gavrin, F. H. Streitz, C. L. Chien, J. J. Rhyne, and J. A. Gotaas, Nature **332**, 238 (1988).

[13]H. Shaked, Jr., J. Faber, B. W. Veal, R. L. Hitterman, and A. P. Paulikas, Solid State Commun. **75**, 445 (1990).

[14]N. Peng, Ph.D. thesis, University of Cambridge, 1992.

[15]M. Mehbod, P. Wyder, R. Deltour, P. H. Duvigneaud, and G. Naessens, Phys. Rev. B **36**, 8819 (1987).

[16]F. J. Blunt, Ph.D. thesis, University of Cambridge, 1990.

[17]A. M. Campbell, J. Phys. C **2**, 1492 (1969).

[18]A. M. Campbell, J. Phys. C **4**, 3186 (1969).

[19]A. M. Campbell, in *Magnetic Susceptibility of Superconductors and Other Spin Systems,* edited by R. A. Hein, T. L. Francavilla, and D. H. Liebenberg (Plenum, New York, 1992).

[20]A. Carrington, A. P. Mackenzie, C. T. Lin, and J. R. Cooper, Phys. Rev. Lett. **69**, 2855 (1992).

[21]A. Porch, H. M. Cheah, and J. R. Waldram, Physica B **165-166**, 1199 (1990).

[22]D. Shoenberg, *Superconductivity* (Cambridge University Press, United Kingdom, 1960).

[23]S. M. Anlage, H. Sze, H. J. Snortland, S. Tahara, B. Langley, C. B. Eom, M. R. Beasley, and R. Taber, Appl. Phys. Lett. **54**, 2710 (1989).

[24]J. R. Cooper, C. T. Chu, L. W. Zhou, B. Dunn, and G. Grüner, Phys. Rev. B **37**, 638 (1988).

[25]L. Krusin-Elbaum, R. J. Green, F. Holtzberg, A. P. Malozemoff, and Y. Yeshurun, Phys. Rev. Lett. **62**, 217 (1989).

[26]S. Mitra, J. H. Cho, W. C. Lee, D. C. Johnston, and V. K. Kogan, Phys. Rev. B **40**, 2674 (1989).

[27]D. R. Harshman, L. F. Schneemeyer, J. V. Waszczak, G. Aeppli, R. J. Cava, B. Batlogg, L. W. Rupp, E. J. Ansaldo, and D. L. Williams, Phys. Rev. B **39**, 851 (1989).

[28]U. Welp, W. K. Kowk, G. W. Crabtree, K. G. Vandervoot, and J. Z. Liu, Phys. Rev. Lett. **62**, 1908 (1989).

[29]D. E. Farrell, J. P. Rice, D. M. Ginsberg, and J. Z. Liu, Phys. Rev. Lett. **64**, 1573 (1990).

[30]U. Welp, S. Flesher, W. K. Kwok, R. A. Klemm, V. M. Vinokur, J. Downey, and G. W. Grabtree, in *High Temperature Superconductivity,* edited by S. K. Malik and S. S. Shah (Nova Science, New York, 1992).

[31]A. B. Pippard, Proc. R. Soc. London, Ser. A **216**, 547 (1953).

[32]T. E. Faber and A. B. Pippard, Proc. R. Soc. London, Ser. A **231**, 336 (1955).

[33]H. Adrian, W. Assmus, A. Hohr, J. Kadewski, H. Spille, and F. Steglich, Physica C **162-164**, 329 (1989).

[34]A. Umezawa, G. W. Crabtree, K. G. Vandervoot, U. Welp, W. K. Kowk, and J. Z. Liu, Physica C **162-164**, 733 (1989).

[35]M. Wacenovsky, H. W. Weber, O. B. Hyun, D. K. Finnemore, and K. Mereiter, Physica C **160**, 55 (1989).

[36]V. N. Kopylov and I. F. Schegolev, Physica C **162-164**, 1143 (1989).

[37]M. Sato, S. Shamoto, M. Sera, and H. Fujishita, Solid State Commun. **72**, 689 (1989).

[38]J. P. Strobel, A. Thoma, B. Hensel, H. Adrian, and K. Saeman-Ischenco Physica C **153-155**, 1537 (1988).

[39]T. Koyama, N. Takezawa, and M. Tachiki, Physica B **165-166**, 1105 (1990).

[40]D. S. Hirashima and T. Matsuura, J. Phys. Soc. Jpn. **59**, 24 (1990).

[41]M. Naito, A. Matsuda, K. Kitazawa, S. Kambe, I. Tanaka, and H. Kojima, Phys. Rev. B **41**, 4823 (1990).

[42]A. S. Aleksandrov and D. A. Samachenko, Zh. Eksp. Teor. Fiz. **99**, 574 (1991) [Sov. Phys. JETP **72**, 321 (1991)].

[43]A. Porch, J. R. Cooper, H. M. Cheah, J. S. Edmends, and J. R. Waldram, Physica B **165-166**, 1199 (1990).

[44]N. R. Werthamer, E. Helfand, and P. C. Hohenberg, Phys. Rev. **147**, 295 (1966).

[45]M. Tinkham and C. J. Lobb, *Solid State Physics* (Academic, New York, 1989), Vol. 42, p. 91.

[46]J. R. Clem, Physica C **153-155**, 50 (1988).

[47]C. P. Bean, Rev. Mod. Phys. **36**, 31 (1964).

[48]H. W. Weber, H. P. Wiesinger, W. Kritscha, and F. M. Sauerzopf, Supercond. Sci. Technol. **4**, S301 (1990).

[49]L. Civale, A. D. Marwick, M. W. McElfresh, T. K. Worthington, A. P. Malozemoff, F. H. Holtzberg, J. R. Thompson, and M. A. Kirk, Phys. Rev. Lett. **65**, 1164 (1990).

[50]L. Civale, A. D. Marwick, T. K. Worthington, M. A. Kirk, J. R. Thompson, L. Krusin-Elbaum, Y. Sun, and F. Holtzberg, Phys. Rev. Lett. **67**, 648 (1991).

[51]M. Murakami, Supercond. Sci. Technol. **5**, 185 (1992).

[52]J. R. Clem, Phys. Rev. B **43**, 7837 (1991).

[53]D. H. Kim, K. E. Gray, R. T. Kampwirth, J. C. Smith, P. Richeson, T. J. Marks, and M. Eddy, Physica C **193**, 67 (1991).

[54]R. S. Liu, D. N. Zheng, J. W. Loram, K. A. Mirza, A. M. Campbell, and P. P. Edwards, Appl. Phys. Lett. **36**, 31 (1992).